STRUCTURAL BIOLOGY COMMUNICATIONS

ISSN 2053-230X

Characterization and 1.57 Å resolution structure of the key fire blight phosphatase AmsI from *Erwinia amylovora*

Marco Salomone-Stagni,[a] Francesco Musiani[b] and Stefano Benini[a]*

[a]Faculty of Science and Technology, Free University of Bozen-Bolzano, Piazza Università 5, 39100 Bolzano, Italy, and [b]Department of Pharmacy and Biotechnology, University of Bologna, Viale G. Fanin 40, 40127 Bologna, Italy. *Correspondence e-mail: stefano.benini@unibz.it

Received 17 October 2016
Accepted 23 November 2016

Edited by Z. Dauter, Argonne National Laboratory, USA

Keywords: hydrolases; amylovoran; low-molecular-weight protein tyrosine phosphatase; kinetics; fire blight; Enterobacteriaceae; *Erwinia amylovora*.

PDB reference: AmsI, 4d74

Supporting information: this article has supporting information at journals.iucr.org/f

AmsI is a low-molecular-weight protein tyrosine phosphatase that regulates the production of amylovoran in the Gram-negative bacterium *Erwinia amylovora*, a specific pathogen of rosaceous plants such as apple, pear and quince. Amylovoran is an exopolysaccharide that is necessary for successful infection. In order to shed light on AmsI, its structure was solved at 1.57 Å resolution at the same pH as its highest measured activity (pH 5.5). In the active site, a water molecule, bridging between the catalytic Arg15 and the reaction-product analogue sulfate, might be representative of the water molecule attacking the phospho-cysteine intermediate in the second step of the reaction mechanism.

1. Introduction

Fire blight is a devastating disease affecting rosaceous plants such as apple, pear and quince (Vanneste, 2000). The Gram-negative bacterium *Erwinia amylovora* is the aetiological agent of the disease. Currently, the main methods to control fire blight are the use of biological and chemical pesticides, antibiotics and resistant cultivars obtained through classical breeding or genetic engineering. Infected cultivars commonly require quarantine, pruning and/or eradication of the plants (Gusberti *et al.*, 2015). Within the *E. amylovora* genome, the *ams* operon is necessary for pathogenicity and is responsible for the synthesis of amylovoran (Bugert & Geider, 1995), which is a complex branched heteropolysaccharide that is essential for virulence and pathogenicity, and is the major component of the exopolysaccharide (EPS) capsule of the bacterium together with levan (Caputi, Cianci *et al.*, 2013; Caputi, Nepogodiev *et al.*, 2013; Geier & Geider, 1993; Nimtz *et al.*, 1996; Bernhard *et al.*, 1993; Wuerges *et al.*, 2015).

The AmsI protein, encoded by the *ams*I gene, is a cytoplasmatic key enzyme of amylovoran metabolism, and thus a potential drug target for the control of fire blight. A balanced amount of AmsI is essential for the synthesis of amylovoran. Overproduction of AmsI leads to considerable inhibition of EPS synthesis, while the *ams*I knockout is deficient in EPS (Bellemann & Geider, 1992; Bugert & Geider, 1995, 1997). AmsI is a cysteine-based protein tyrosine phosphatase (PTP). PTPs putatively catalyse the dephosphorylation of a cognate kinase on phospho-tyrosine residues. The kinase–phosphatase dual system plays a critical role in bacterial virulence and cell

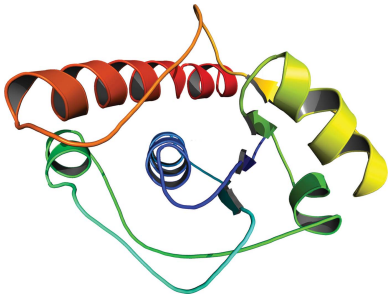

signalling (Bechet *et al.*, 2009; Byrne *et al.*, 2011; Cozzone *et al.*, 2004; Grangeasse *et al.*, 2007, 2010, 2012; Kolot *et al.*, 2008; Lacour *et al.*, 2008; Morona *et al.*, 2006; O'Riordan & Lee, 2004). In particular, their involvement in the synthesis and export of polysaccharides responsible for biofilm and capsule formation, antibiotic resistance, lysogenization and DNA metabolism has been demonstrated. PTPs can be divided into three families: high-molecular-weight PTPs (HMW-PTPs; receptor-like and nonreceptor), dual-specificity PTPs (DS-PTPs; specificity for phospho-tyrosine and phospho-serine/threonine) and low-molecular-weight PTPs (LMW-PTPs), with a molecular mass of about 18 kDa (Walton & Dixon, 1993; Charbonneau & Tonks, 1992; Tabernero *et al.*, 2008; Zhang & Dixon, 1994; Blenis, 1993; Yuvaniyama *et al.*, 1996; Denu *et al.*, 1995; Zhang *et al.*, 1995; Raugei *et al.*, 2002; Caselli *et al.*, 2016). The three PTP families share no sequence homology apart from a signature motif C(X)$_5$R(S/T) contributing to the phosphate-binding loop (P-loop) in the active site and a catalytic aspartate residue followed by a proline and often a tyrosine, which are part of the so-called D-loop.

AmsI is a member of the LMW-PTPs, which are found both in prokarya and eukarya (Su *et al.*, 1994; Tabernero *et al.*, 2008; Zhang, Van Etten *et al.*, 1994; Zhang *et al.*, 1997, 1998; Zabell *et al.*, 2006; Stehle *et al.*, 2012; Wang *et al.*, 2000; Lescop *et al.*, 2006; Madhurantakam *et al.*, 2005; Vega *et al.*, 2011; Gustafson *et al.*, 2005; Hagelueken *et al.*, 2009; Xu *et al.*, 2006). The LMW-PTPs share a conserved P-loop motif consisting of a CXGNXCRSP consensus sequence, where X corresponds to a leucine, isoleucine, threonine or phenylalanine residue (see the alignment in Fig. 1).

From a structural point of view there are strong similarities among all of the LMW-PTPs. They share an overall fold, the P-loop in the N-terminal region and the same catalytic residues. Significant variability is observed among the residues forming the protein surface around the active site, and it is becoming clear that these residues have great importance in

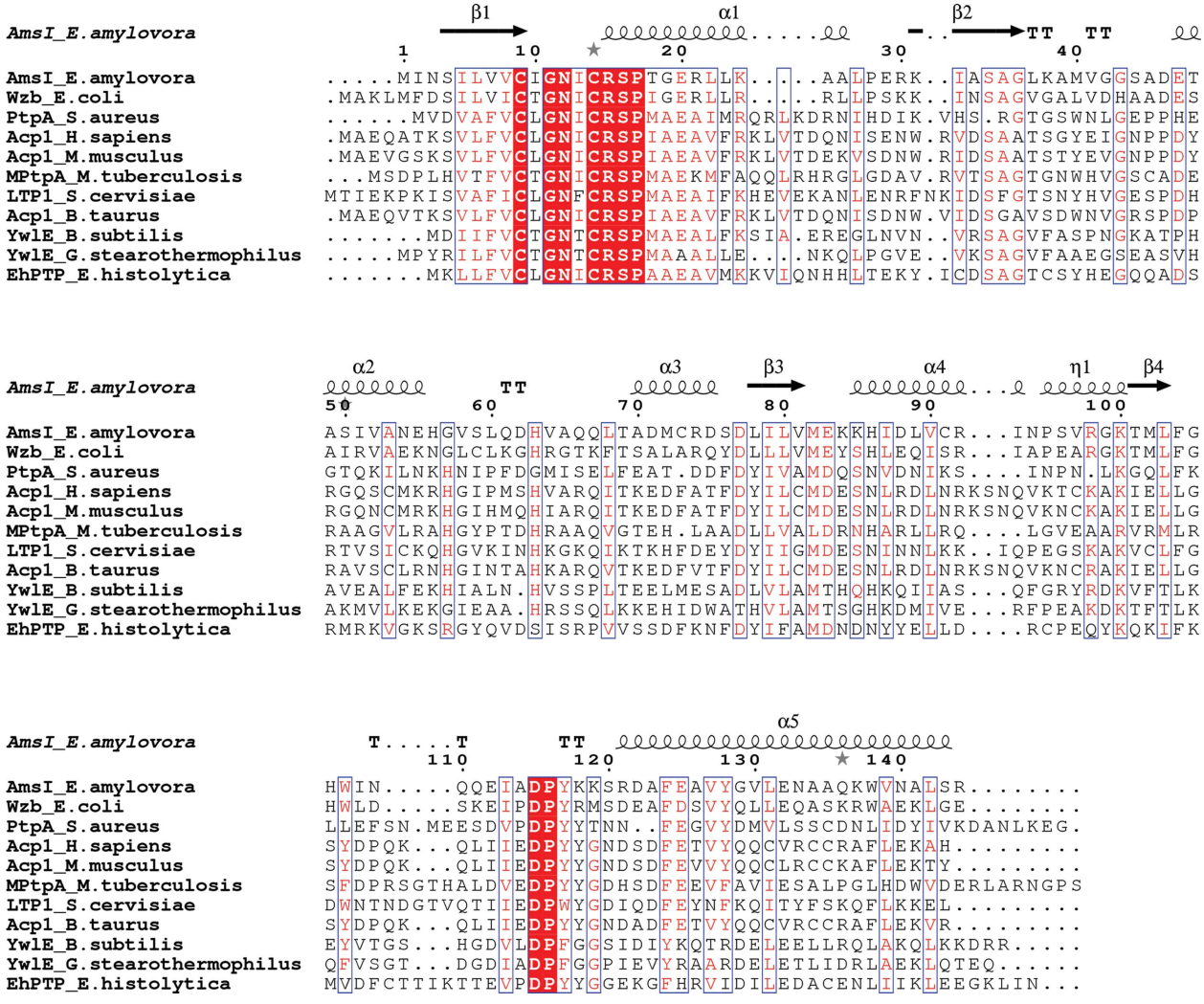

Figure 1
Alignment of LMW-PTPs. Sequence alignment of LMW-PTPs for which X-ray diffraction structures are available (the sequence names consist of the protein name followed by the source organism). The secondary-structural elements in AmsI are shown at the top. Conserved residues are highlighted in red. The characters in red represent the conservative residues. This figure was created using the *ESPript* server (Robert & Gouet, 2014).

the interaction with the cognate kinase, such as the central positions of the W-loop (Grangeasse *et al.*, 2003; Temel *et al.*, 2013; Bechet *et al.*, 2010). The structural determination of the interaction between Wzb (an analogue of AmsI) and Wzc (an analogue of AmsA, the cognate kinase of AmsI) has been described (Temel *et al.*, 2013).

The catalytic mechanism of the LMW-PTPs has been extensively investigated. According to the current model, the reaction starts with the formation of a covalent phospho-enzyme intermediate (Davis *et al.*, 1994). The nucleophile is the S^{γ} atom of a cysteine present in the P-loop. This first step is assisted by the protonation of the leaving group (*i.e.* dephosphorylated protein) O atom by a general acid consisting of the conserved aspartate residue of the D-loop (Zhang & Van Etten, 1991). A P-loop arginine is involved both in substrate binding and in the stabilization of the reaction intermediate (Zhang, Wang *et al.*, 1994). The catalytic cysteine and arginine, together with other residues of the P-loop, form a cradle providing critical hydrogen-bonding interactions with the phosphate group of the substrate, holding it in place for the subsequent nucleophilic attack (Evans *et al.*, 1996). In fact, the amide groups in the P-loop point towards the interior of the cradle and form a network of hydrogen bonds with the phosphate O atoms. During the second step, which is the rate-limiting step, the phospho-cysteine intermediate is attacked by a water molecule. The same aspartate that acted as a general acid in the first step serves as a general base during hydrolysis of the phospho-enzyme by accepting a proton from the water molecule and by assisting the conversion of the phospho-cysteine enzyme to its resting state, regenerating the free enzyme (Zhang, Harms *et al.*, 1994; Denu & Dixon, 1995; Denu *et al.*, 1996). Finally, inorganic phosphate is released from the enzyme.

In order to investigate the key fire blight phosphatase AmsI, we solved its crystal structure at 1.57 Å resolution, we studied its oligomerization state using static light scattering and we studied its activity using steady-state kinetic analysis.

2. Materials and methods

2.1. Macromolecule production

Chemicals were purchased from Sigma–Aldrich unless stated otherwise. AmsI (UniProt D4I6U1_ERWAE; EC 3.1.3.48) from *E. amylovora* (strain ATCC 49946/CCPPB 0273/Ea273/27-3) was cloned, expressed and purified as described previously (Benini *et al.*, 2014). Briefly, the *amsI* gene was amplified by PCR from the genomic DNA and inserted into a pETM-11 (EMBL) vector that fuses an N-terminal His_6 tag and a TEV protease cleavage site to the N-terminus of the protein (Dümmler *et al.*, 2005). AmsI was expressed in *Escherichia coli* strain BL21 (DE3). The purification consisted of two strategies, depending on whether protein with or without the tag was needed. To obtain protein with the tag, immobilized metal-affinity chromatography (IMAC) was followed by size-exclusion chromatography (SEC). To obtain protein without the tag, an initial IMAC step, TEV protease cleavage, buffer exchange with a HiPrep 26/10 column (when only buffer exchange is required, this enables the process to be sped up and the loss of protein to be decreased with respect to size exclusion), a second IMAC step and a final SEC step. The obtained final fractions were in 20 m*M* Tris–HCl pH 7.5, 150 m*M* NaCl, 0.5 m*M* TCEP. For crystallization purposes, the fractions were pooled and concentrated to 15 mg ml^{-1} by ultrafiltration using a Vivaspin 20 Centricon with 5 kDa cutoff (Sartorius). In order to compare the elution profiles of AmsI with and without the histidine tag, we ran analytical size-exclusion chromatography using a Superdex 75 10/300 GL column (GE Healthcare, Sweden) in 20 m*M* HEPES pH 7.5, 150 m*M* NaCl, 2 m*M* TCEP at room temperature.

2.2. Crystallization

AmsI was crystallized from a 15 mg ml^{-1} protein solution using a microbatch-under-oil setup at 293 K in 96-well MRC plates (Molecular Dimensions) and volatile oil, as described previously (Benini *et al.*, 2014).

The crystallization wells were protected from drying using adhesive ClearView sheets (Molecular Dimensions). Drops of 1 µl precipitant solution were added to 15 µl volatile oil, immediately followed by 1 µl protein solution. Crystals grew within two weeks to maximum dimensions of about 0.2 × 0.2 × 0.2 mm in 1.7 *M* ammonium sulfate, 100 m*M* sodium acetate pH 5.5. Crystals were obtained using the His_6-tagged AmsI.

2.3. Data collection and processing

Diffraction data were collected at 100 K on a Dectris PILATUS 6M detector on EMBL beamline P13 (PETRA III, DESY, Hamburg, Germany). The wavelength was set to 1.033 Å. The data were processed using *XDS* (Kabsch, 2010). Space-group determination was carried out using *POINTLESS* (Evans, 2011) and the data were scaled with *AIMLESS* (Evans, 2006). The crystal belonged to space group $P3_121$ and diffracted to a maximum resolution of 1.57 Å (Benini *et al.*, 2014).

2.4. Structure solution and refinement

The structure was solved by molecular replacement using *BALBES* (Long *et al.*, 2008). *BALBES* automatically searched the PDB and found the *E. coli* LMW-PTP Wzb (PDB entry 2wmy; 51% sequence identity; Hagelueken *et al.*, 2009) to be the best model for molecular replacement. Model building was carried out and water molecules were added using *Coot* (Emsley *et al.*, 2010). The structure was refined with *REFMAC*5 to a final R and R_{free} of 0.169 and 0.179, respectively. The asymmetric unit contains one molecule of AmsI with a solvent content of 55.36% and a Matthews coefficient of 2.75 $Å^3$ Da^{-1}. Table 1 reports a summary of refinement and model quality (PDB entry 4d74).

2.5. Static light-scattering experiments (SEC-QELS)

SLS measurements were carried out using a Wyatt QELS apparatus (Dawn EOS, Wyatt Technology) coupled to an

HPLC pump (Knauer Smartline Pump 1000). The SLS device was equipped with a laser beam operating at λ = 690 nm. Light-scattering intensities recorded at 18 angles between 14.2 and 163.5° were obtained using the *ASTRA* software with a gyration radius of between 0.5 and 10 nm. This procedure consists of plotting Kc/R_θ versus $\sin^2(\theta/2) + kc$, where K is an optical constant which contains the specific refractive-index increment dn/dc (0.18 ml g^{-1} in this case), c is the concentration of protein (g ml^{-1}), R_θ is the Rayleigh ratio, k is a constant for the graphical representation of the Zimm diagram and θ is the angle of observation. Extrapolations to zero angle and concentration provided the values of molecular mass and $R_{g,z}$.

To study the oligomerization state of the protein, AmsI deprived of the His_6 tag was assessed at concentrations ranging from 2 to 20 mg ml^{-1} in the presence and absence of 5 m*M* sulfate ion. The sulfate ion was used to evaluate its contribution to the dimerization observed in the crystal structure. In order to separate and analyse different-sized species present in solution, a Superdex 75 10 300 GL column connected to the HPLC pump was used. The running-buffer formulations were 20 m*M* Tris–HCl, 150 m*M* NaCl, 2 m*M* TCEP and, alternatively, the same buffer with the addition of 5 m*M* sodium sulfate. The buffers were extensively filtered and degassed. The pure protein was centrifuged at 16 000*g* for 15 min at 4°C before experiments and 100 µl was injected into the column.

2.6. Steady-state kinetics

The protein used in all of the experiments derived from the same batch as utilized for crystallization and structure determination. AmsI showed a purity of greater than 99% as indicated by SDS–PAGE analysis. The activity of AmsI was studied by stopped-assay steady-state kinetic experiments (Gardossi *et al.*, 2010; Bisswanger, 2011, 2014; Tipton *et al.*, 2014) following the formation of *p*-nitrophenyl (*p*NP) from the hydrolysis of *p*-nitrophenyl phosphate (*p*NPP) at 405 nm using an ε_c of 18 000 M^{-1} cm^{-1} (Davis *et al.*, 1994). The quantification of *p*NP was calculated using a path length of 0.65 cm, corresponding to 250 µl of solution in a well of 3.48 mm radius, as stated by the plate-manufacturing company (VWR International). The errors on V_{max} and K_m were calculated as standard deviations by *GraphPad Prism* v.5.03 (GraphPad Software). The relative statistical error propagation was taken into account and errors were rounded in excess.

Experiments were carried out at 25°C using 100 m*M* buffers: citrate pH 4.8, citrate pH 5.5, citrate pH 6.5 and bicine pH 8.5. The reactions were set up in transparent 96-well plates (Greiner Bio-One, VWR International, USA). The total reaction volume per well was 200 µl. For each buffer, an experiment consisting of 96 conditions was carried out at least in triplicate. For each experiment, 12 substrate concentrations were used ranging from 0.5 to 30 m*M* and positioned from plate columns 1 to 12. Row A was used for blank solutions where no enzyme was added. Rows B–H were identical and each was used for a different quenching time, giving a total of seven timing points. The reactions were started by the addition of 20 µl enzyme prepared by the dilution of a 20 mg ml^{-1} solution in the same buffer as the experiment. The enzyme concentration was 50 ng ml^{-1} (2.65 n*M*) and therefore 10 ng was used per well. The protein concentration was estimated in 6 *M* urea by spectrophotometry using the parameters M_r = 19 kDa and ε_c = 17 mM^{-1} cm^{-1} as estimated by *ProtParam* (Gasteiger *et al.*, 2005). The reactions were quenched by adding 50 µl 1 *M* NaOH to a final concentration of 0.2 *M*. The pH increase owing to NaOH also enhances the *p*NP colour development, as accurate measurement requires that the 4-nitrophenol product is fully deprotonated.

The 96-well plates were read using a Tecan Infinite 200 PRO (Tecan Group AG, Männedorf, Switzerland) immediately after the end of the experiment and also the day after to check that no changes owing to incomplete colour development or incomplete quenching occurred (no difference was measured). For each protein sample at least nine measurements were taken and the resulting values were averaged. Every well was read in four different positions using 25 flashes per reading point and the values were then averaged out. The exclusion of one reading point was allowed when it was not consistent with the other three.

Table 1
Structure solution and refinement.

Values in parentheses are for the outer shell.

Resolution range (Å)	57.18–1.57 (1.611–1.570)
Completeness (%)	99.9
No. of reflections, working set	24575 (1785)
No. of reflections, test set	1318 (97)
Final R_{cryst}	0.169 (0.208)
Final R_{free}†	0.179 (0.232)
Cruickshank DPI‡	0.069
No. of non-H atoms	
Protein	1157
Ion	15
Ligand	0
Water	100
Total	1272
R.m.s. deviations	
Bonds (Å)	0.012
Angles (°)	1.591
Average B factors (Å^2)	
Protein	23.1
Ion	37.7
Ligand	0.0
Water	31.2
Ramachandran plot	
Most favoured (%)	96
Allowed (%)	4

† To calculate R_{free}, a subset of reflections (5.0%) was randomly chosen as a test set. ‡ Diffraction-component precision indicator of the atom position.

3. Results and discussion

3.1. Tertiary structure

The X-ray diffraction structure of AmsI from *E. amylovora* was solved at 1.57 Å resolution (final R = 0.16; R_{free} = 0.17; see Table 1 for refinement statistics) in complex with the product analogue sulfate (PDB entry 4d74).

The residue numbering in the PDB file starts at −7. Residues −7 to −1 correspond to the TEV cleavage site that is part of the N-terminal His_6 fusion tag. No electron density was visible for the first 12 residues owing to disorder or multiple conformations. The N-terminus is opposite the active site and has been reported not to influence catalysis (Ostanin *et al.*, 1995; Wang *et al.*, 2000). Residue 1 corresponds to the first amino acid of the wild-type sequence and residue 2 is a conservative mutation Ile to Val as a consequence of the cloning strategy.

The enzyme has the typical $\beta\alpha\beta$ fold of the LMW-PTPs characterized by $\beta1\alpha1\beta2$ and $\beta3\alpha4\beta4$ motifs that create a central four-stranded β-sheet (Fig. 2).

This β-sheet together with helices $\alpha1$, $\alpha2$ and $\alpha5$ sets up the hydrophobic core of the protein. The large hydrophobic moment of helix 5 (calculated with *DS Visualizer* 4.0; Accelrys Software Inc.) indicates its incisive role in AmsI folding (Supplementary Fig. S1). Three long loops characterize the structure: loop $\beta2$–$\alpha2$ (the W-loop), loop $\alpha2$–$\alpha3$ and loop $\beta5$–$\alpha4$ (the D-loop). In particular, the D-loop, connecting $\beta4$ and $\alpha5$ and bearing the conserved catalytic Asp115 and Pro116 residues, is defined by an N-terminal type I β-turn and a C-terminal type II β-turn and is kept stretched by its interactions with helix $\alpha5$. The overall fold of AmsI is very well conserved among the LMW-PTPs (a three-dimensional representation of their structural conservation is available as Supplementary Fig. S2). *E. coli* Wzb (PDB entry 2wmy; 51% sequence identity) is the structure closest to AmsI, with an r.m.s.d. of 0.8 Å.

No residues were found in disallowed regions of the Ramachandran plot (Supplementary Fig S3). Asn12 adopts a left-handed conformation, which is a conserved feature of the P-loop. Asp62 and Lys118 are also in a left-handed conformation and are part of the long loop connecting helices $\alpha2$ and $\alpha3$ and of the turn connecting $\alpha5$ and the D-loop, respectively. Pro95, Ser96 and Val97 form a 3_{10}-helix turn and are part of the portion of the protein connecting helix $\alpha4$ and strand $\beta4$. The dihedral angles of the central amino acids in the D-loop (residues 112–117) are in a β-strand conformation, apart from Pro116, which is located in the α-helical region of the Ramachandran plot.

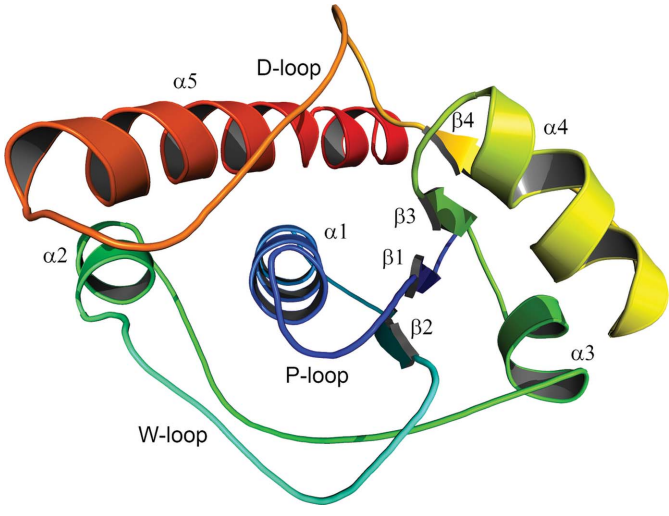

Figure 2
AmsI structure. Cartoon representation of the *E. amylovora* low-molecular-weight protein tyrosine phosphatase AmsI. The secondary-structure elements are named and coloured according to their N- to C-terminal position within the protein chain (*e.g.* from $\alpha1$ to $\alpha5$). This image was prepared with the *PyMOL* molecular-graphics system (v.1.7; Schrödinger).

The thermal displacements (*B* factors) of the structure were refined isotropically. The protein mean isotropic displacement (ID) is 23.1 $Å^2$. As expected, the sulfate and the water in the active site show higher displacements of about 26.7 and 33.5 $Å^2$, respectively. Not surprisingly, the highest IDs were found for an arginine and for a lysine residue: Arg92 (ID = 46.87 $Å^2$) is part of helix $\alpha4$ and Lys118 (ID = 43.45 $Å^2$) is part of the turn that ends at helix $\alpha5$.

3.2. Quaternary structure

In the crystallographic unit cell, the AmsI monomer is packed in a dimeric form by symmetry. Considering only the native residues, upon dimerization each monomer has a buried surface of about 424 $Å^2$ from a total monomer surface of about 7465 $Å^2$, as calculated by the *PBDePISA* server (Krissinel & Henrick, 2007; CSS score = 0.03; the complexation significance score, CSS, scores how significant the interface is for assembly formation). The buried area accounts for about 6% of the surface of each AmsI monomer. Considering that the interaction surfaces in protein complexes range from ∼600 to ∼4800 $Å^2$ (representing 6–24% of the accessible surface area of the individual monomers, with an average of about 12%), the stability of the AmsI dimer appears to be weak (Janin *et al.*, 1988; Kleanthous, 2000). It is worth noting that a sulfate anion, the purification tag (residues Gln−2, Tyr−4, Phe−3) and residues Lys84 and Asp109 contribute to the monomer–monomer interaction. Hence, in order to evaluate the oligomerization state of AmsI in solution, SEC-QELS experiments at different concentrations of AmsI without a His_6 tag in the absence and presence of sulfate were carried out. The AmsI samples were highly monodisperse. The molecular mass was calculated to be about 16 kDa and the $R_{g,z}$ about 1.8 nm for every measured sample. The results reveal that in each case AmsI elutes as a monomer in solution (Supplementary Fig. S4, Supplementary Table S1). Moreover, comparing the analytical size-exclusion chromatography elution profiles of AmsI with and without the tag it is clear that His_6-tagged AmsI is also a monomer in solution (Supplementary Fig. S5).

3.3. Active site

The active site is located in a crevice directly exposed to the solvent. The P-loop forms half of the active site and contains part of the consensus sequence $C(X)_5R(S/T)$, here ^{9}CIGNICRS[16], which is putatively responsible for interacting with the phosphoryl moiety of the substrate (Fig. 3). In fact, residues Cys9–Ser16 bind a sulfate molecule that keeps AmsI in a closed conformation (Tabernero *et al.*, 2008), in contrast to the

open conformation observed in a homologous structure when no ligand is present (Stehle *et al.*, 2012).

The P-loop binds the sulfate O atoms through its peptidic amino groups. The P-loop is further stabilized by a hydrogen-bond network with residues 18–20, 34–40, Asp46 and His63. The conserved Asn12 shows the typical left-handed conformation stabilized by either the P-loop or by hydrogen bonds to His63 N^{ε}, Ser34 O^{γ}, Gln66 N and Ser16 O^{γ}. The Arg15 side chain binds the P-loop backbone O atom of Ile113 and Glu83 O^{ε}. The conserved Cys14 features two distinct conformations (modelled with 50% occupancy each), both pointing away from the phosphate pocket. The amino acids involved in catalysis are highly conserved and consist of Cys9, Arg15 and Asp115. Arg15 is a strictly conserved catalytic residue and has been shown to be involved in the binding of sulfate/phosphate O atoms (Wang *et al.*, 2000; Zhang *et al.*, 1997, 1998; Hagelueken *et al.*, 2009; Lescop *et al.*, 2006; Stehle *et al.*, 2012). Interestingly, we observed an electron density that was undoubtedly modelled as a water molecule (HOH2017 in the PDB entry; a figure showing the active site with electron density is available as Supplementary Fig. S6) bridging Arg15 and the sulfate, which are shifted 1.2–1.6 Å apart compared with the corresponding arginine and sulfates or phosphates of the other reported X-ray diffraction structures (see Supplementary Fig. S7). This is also reflected in the main difference observed in the P-loop between AmsI and *E. coli* Wzb. Wzb Cys13 (the residue affording the phospho-cysteine intermediate during the reaction) points towards the sulfate, while in AmsI the corresponding Cys9 points away from the sulfate as it is otherwise too close. The HOH2017 molecule makes hydrogen bonds to both the sulfate O atoms and the Arg15 N^{ε} and backbone N atoms, and it is 3.5 Å from the O^{δ} atom of Asp115, which is the acid–base catalyst of the reaction.

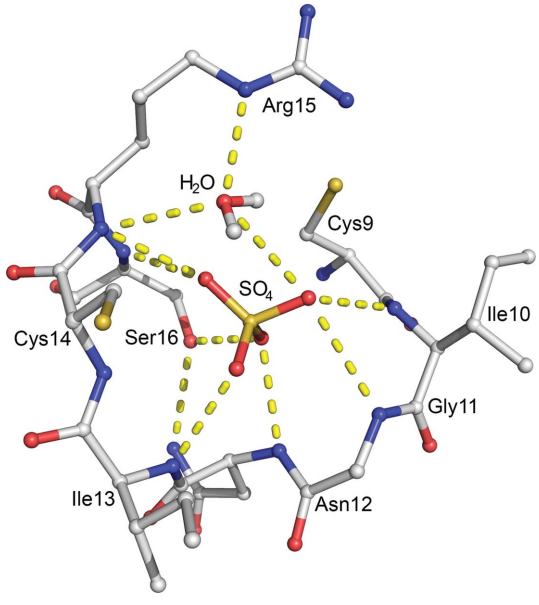

Figure 3
AmsI active site. Residues 10–16 of the P-loop, the sulfate (SO_4) and the water molecule (H_2O; HOH2017) in the active site are shown in ball-and-stick representation. Atoms are coloured as follows: carbon, grey; oxygen, red; nitrogen, blue; sulfur, yellow; hydrogen, white. The water H atoms are included in the model. Hydrogen bonds are represented as dotted yellow lines. This image was prepared with the *PyMOL* molecular-graphics system (v.1.7; Schrödinger).

Table 2
Kinetic parameters of AmsI.

Measurements were taken at 25°C, in 200 µl reaction volumes, using 2.65 n*M* protein and *p*NPP as substrate.

Buffer (100 m*M*)	pH	Calculated ionic strength (m*M*)	K_m (m*M*)	k_{cat} (s^{-1})	k_{cat}/K_m ($\times 10^{-3}$ M^{-1} s^{-1})	Fit R^2
Citrate	5.5	235	1.3 ± 0.2	34.4 ± 0.8	28 ± 5	0.97
Citrate	6.5	248	1.9 ± 0.4	10.0 ± 0.4	5 ± 2	0.93
Bicine	8.5	44	10 ± 4	0.8 ± 0.1	0.08 ± 0.03	0.92

Asp115 forms a hydrogen bond through its $O^{\delta 1}$ atom to the backbone N atom of Tyr117; it is placed parallel to the guanidinium group of Arg15 and establishes electrostatic interactions with it. In eukarya, the residue corresponding to Tyr117 is followed by another tyrosine that is involved in the regulation by phosphorylation (Tabernero *et al.*, 2008). In AmsI Tyr117 is uniquely followed by two lysine residues that could be involved in the interaction with the cognate kinases. In AmsI, Met40 plays a corresponding role to the Tyr/Trp residue of the studied eukaryotic LMW-PTPs (*e.g.* Tyr49 in human Acp1). The entrance to the active site is dominated by the residues Ile10, Gly11, Ile13, Arg15, Met40, Asp115 and Tyr117. These amino acids form a doughnut-like structure around the entrance. Half of this structure is formed by polar residues, while the other half is formed by hydrophobic residues (Supplementary Fig. S8*a*). A similar pattern characterizes the entire protein surface around the active site (Supplementary Fig. S8*b*). Specifically, the polar part is characterized by Glu83, **Lys85**, Asp115, **Tyr117**, **Lys118** and **Lys119**, while the hydrophobic moiety by the residues Ile10, **Gly11**, Leu37, **Met40** and **Val41**. Interestingly, the hydrophobic area around the active site is interrupted by **Lys38** protruding from the middle. According to our docking model, the residues in bold above are important for the AmsI–AmsA interaction.

3.4. AmsI kinetics

Stopped-assay steady-state kinetic experiments were carried out at 25°C using *para*-nitrophenyl phosphate (*p*NPP) as a substrate (Table 2).

Three acidic pH values and one basic condition were tested. Below pH 5 the proteins tended to aggregate and precipitate, no matter which buffer was used (data not shown). In citrate at pH 5.5 AmsI showed a k_{cat} of 34.4 s^{-1} and a k_{cat}/K_m of 28×10^{-3} M^{-1} s^{-1}. Citrate at pH 6.5 gave a k_{cat} of 10.0 s^{-1} and a k_{cat}/K_m of 5×10^{-3} M^{-1} s^{-1}. As expected from an acidic phosphatase, AmsI showed a lower activity rate in bicine at pH 8.5, with a k_{cat} of 0.8 s^{-1}.

4. Discussion and conclusions

Fire blight is a major global threat to commercial apple and pear production and is caused by the bacterium *E. amylovora*,

which has been included in the top ten plant pathogenic bacteria (Mansfield *et al.*, 2012). AmsI is an LMW-PTP that is necessary for *E. amylovora* pathogenicity by regulating the biosynthesis of the pathogenicity factor amylovoran. AmsI folds into a structure akin to all other known LMW-PTPs, emphasizing the high structural conservation in this type of phosphatase (Su *et al.*, 1994; Tabernero *et al.*, 2008; Zhang, Van Etten *et al.*, 1994; Zhang *et al.*, 1997, 1998; Zabell *et al.*, 2006; Stehle *et al.*, 2012; Wang *et al.*, 2000; Lescop *et al.*, 2006; Madhurantakam *et al.*, 2005; Vega *et al.*, 2011; Gustafson *et al.*, 2005; Hagelueken *et al.*, 2009; Xu *et al.*, 2006). The oligomerization state of LMW-PTPs has been debated for a long time, and it is thought to regulate the enzymatic activity by competing with the substrate (Blobel *et al.*, 2009). The dominant oligomerization process is the formation of dimers. In mammalian LMW-PTPs, the active monomers are in equilibrium with inactive dimers (Tabernero *et al.*, 1999; Åkerud *et al.*, 2002; Blobel *et al.*, 2009). In prokaryotic LMW-PTPs, weak dimerization has been reported for *E. coli* Wzb, *Bacillus subtilis* YwlE and *Staphylococcus aureus* PtpB (Nath *et al.*, 2014). In general, dimerization inactivates the enzyme and involves residues in the active site and tyrosines in the D-loop. Recently, Nath and coworkers revealed that VcLMWPTP from *Vibrio cholerae* dimerizes in a novel fashion, involving new interactions and leaving the enzyme active (Nath *et al.*, 2014). AmsI is present as a dimer in the crystal unit cell, with a previously unreported dimerization interface which involves part of the His_6 tag and a sulfate ion. However, we demonstrate that AmsI is a permanent fully active monomer in solution and that the dimer is a crystal-packing artefact that is not functionally relevant.

In the AmsI active-site pocket a water molecule bridges the catalytic arginine and the sulfate. Such a scenario has only been proposed for the NMR structure of *B. subtilis* YwlE and is not observed in the structures of other homologues (Xu *et al.*, 2006). In contrast to the other LMW-PTP structural models, the sulfate in AmsI is more deeply nestled within the P-loop and is further from the Arg15 side chain. In our scenario, in which it is in close proximity to both the sulfate and the catalytic cysteine, could the water molecule be representative of that attacking the phospho-Cys9 during the second step of the reaction? In fact, during this step Arg15 may act as the base, abstracting a proton from the water and favouring the hydrolysis of the phospho-Cys9 intermediate phospho-thionate bond. Afterwards, Arg15 could donate the proton to the nearby Asp115. Further studies will be needed to address this hypothesis.

In AmsI the sulfate binds to the P-loop residues C$\boldsymbol{X_5}$RS (bold), to the abovementioned water molecule and to the side-chain O atom and the backbone N atom of the P-loop Ser16. This situation is not observed in the homologous LMW-PTPs, where the ligand is bound to Arg N^{ε}, Arg $N^{\eta 2}$ and sometimes to the catalytic cysteine. Another exception is found in *Entamoeba histocolytica* EhPTP, where there is a sulfate ligand bound both to the P-loop serine and the catalytic cysteine.

The kinetic study of AmsI shows a decay in activity at basic pH. In the conditions used in this study citrate pH 5.5 is the optimal buffer. This observation is consistent with the results obtained for other LMW-PTPs, such as those from *B. subtilis*, *S. aureus* and *Yersinia enterocolitica*, with the best conditions at pH 5.5–6.0, 6.2 and 5.5, respectively (Zhang, Wang *et al.*, 1994; Musumeci *et al.*, 2005; Soulat *et al.*, 2002).

Structural and mutational studies on the AmsI–AmsA complex are planned to understand the protein–protein interaction between the two partners. To provide a hint towards a potential model of the interaction, we performed homology modelling of the AmsI cognate kinase AmsA, and based on the data published by Temel *et al.* (2013), and new partial data from the same group, we identified potential putative interaction patches on the surface of the two proteins. This information can be found in the Supporting Information (§S2, Supplementary Tables S2 and S3, Supplementary Figs. S9, S10, S11 and S12).

Acknowledgements

We thank Dr M. Malnoy (Fondazione Edmund Mach, S. Michele all'Adige, Trento, Italy) for providing the genomic DNA from *E. amylovora* strain Ea273. We thank Professor R. Ghose of the Department of Chemistry and Biochemistry of the City College of New York for supplying the experimental NMR data used in the docking simulation. We thank the CERM (Centro di Risonanze Magnetiche), Sesto Fiorentino, Italy for making available the QELS facility, with special regard to Dr Leonardo Gonnelli for his precious help with QELS measurements and data analysis. Plasmid pETM-11 was obtained from the European Molecular Biology Laboratory under a signed Material Transfer Agreement. Data were collected under the European Molecular Biology Laboratory beam time award No. MX-152. The work was supported by the Fondazione Libera Università di Bolzano and by the Autonomous Province of Bolzano project: 'A structural genomics approach for the study of the virulence and pathogenesis of *Erwinia amylovora*'. FM was supported by the University of Bologna through the FARB Program (Finanziamenti dell'Alma Mater Studiorum alla Ricerca di Base).

References

Åkerud, T., Thulin, E., Van Etten, R. L. & Akke, M. (2002). *J. Mol. Biol.* **322**, 137–152.
Bechet, E., Gruszczyk, J., Terreux, R., Gueguen-Chaignon, V., Vigouroux, A., Obadia, B., Cozzone, A. J., Nessler, S. & Grangeasse, C. (2010). *Mol. Microbiol.* **77**, 1315–1325.
Bechet, E., Guiral, S., Torres, S., Mijakovic, I., Cozzone, A. J. & Grangeasse, C. (2009). *Amino Acids*, **37**, 499–507.
Bellemann, P. & Geider, K. (1992). *J. Gen. Microbiol.* **138**, 931–940.
Benini, S., Caputi, L. & Cianci, M. (2014). *Acta Cryst.* F**70**, 1693–1696.
Bernhard, F., Coplin, D. L. & Geider, K. (1993). *Mol. Gen. Genet.* **239**, 158–168.
Bisswanger, H. (2011). *Practical Enzymology*, 2nd ed. Weinheim: Wiley-VCH.
Bisswanger, H. (2014). *Perspect. Sci.* **1**, 41–55.
Blenis, J. (1993). *Proc. Natl Acad. Sci. USA*, **90**, 5889–5892.
Blobel, J., Bernadó, P., Xu, H., Jin, C. & Pons, M. (2009). *FEBS J.* **276**, 4346–4357.

Bugert, P. & Geider, K. (1995). *Mol. Microbiol.* **15**, 917–933.
Bugert, P. & Geider, K. (1997). *FEBS Lett.* **400**, 252–256.
Byrne, J. P., Morona, J. K., Paton, J. C. & Morona, R. (2011). *J. Bacteriol.* **193**, 2341–2346.
Caputi, L., Cianci, M. & Benini, S. (2013). *Acta Cryst.* F**69**, 570–573.
Caputi, L., Nepogodiev, S. A., Malnoy, M., Rejzek, M., Field, R. A. & Benini, S. (2013). *J. Agric. Food Chem.* **61**, 12265–12273.
Caselli, A., Paoli, P., Santi, A., Mugnaioni, C., Toti, A., Camici, G. & Cirri, P. (2016). *Biochim. Biophys. Acta*, **1864**, 1339–1355.
Charbonneau, H. & Tonks, N. K. (1992). *Annu. Rev. Cell Biol.* **8**, 463–493.
Cozzone, A. J., Grangeasse, C., Doublet, P. & Duclos, B. (2004). *Arch. Microbiol.* **181**, 171–181.
Davis, J. P., Zhou, M.-M. & Van Etten, R. L. (1994). *J. Biol. Chem.* **269**, 8734–8740.
Denu, J. M. & Dixon, J. E. (1995). *Proc. Natl Acad. Sci. USA*, **92**, 5910–5914.
Denu, J. M., Lohse, D. L., Vijayalakshmi, J., Saper, M. A. & Dixon, J. E. (1996). *Proc. Natl Acad. Sci. USA*, **93**, 2493–2498.
Denu, J. M., Zhou, G., Guo, Y. & Dixon, J. E. (1995). *Biochemistry*, **34**, 3396–3403.
Dümmler, A., Lawrence, A. M. & de Marco, A. (2005). *Microb. Cell Fact.* **4**, 34.
Emsley, P., Lohkamp, B., Scott, W. G. & Cowtan, K. (2010). *Acta Cryst.* D**66**, 486–501.
Evans, P. (2006). *Acta Cryst.* D**62**, 72–82.
Evans, P. R. (2011). *Acta Cryst.* D**67**, 282–292.
Evans, B., Tishmack, P. A., Pokalsky, C., Zhang, M. & Van Etten, R. L. (1996). *Biochemistry*, **35**, 13609–13617.
Gardossi, L., Poulsen, P. B., Ballesteros, A., Hult, K., Švedas, V. K., Vasić-Rački, Đ., Carrea, G., Magnusson, A., Schmid, A., Wohlgemuth, R. & Halling, P. J. (2010). *Trends Biotechnol.* **28**, 171–180.
Gasteiger, E., Hoogland, C., Gattiker, A., Duvaud, S., Wilkins, M., Appel, R. & Bairoch, A. (2005). *The Proteomics Protocols Handbook*, edited by J. M. Walker, pp. 571–607. Totowa: Humana Press.
Geier, G. & Geider, K. (1993). *Physiol. Mol. Plant Pathol.* **42**, 387–404.
Grangeasse, C., Cozzone, A. J., Deutscher, J. & Mijakovic, I. (2007). *Trends Biochem. Sci.* **32**, 86–94.
Grangeasse, C., Nessler, S. & Mijakovic, I. (2012). *Philos. Trans. R. Soc. B Biol. Sci.* **367**, 2640–2655.
Grangeasse, C., Obadia, B., Mijakovic, I., Deutscher, J., Cozzone, A. J. & Doublet, P. (2003). *J. Biol. Chem.* **278**, 39323–39329.
Grangeasse, C., Terreux, R. & Nessler, S. (2010). *Biochim. Biophys. Acta*, **1804**, 628–634.
Gusberti, M., Klemm, U., Meier, M. S., Maurhofer, M. & Hunger-Glaser, I. (2015). *Int. J. Environ. Res. Publ. Health*, **12**, 11422–11447.
Gustafson, C. L., Stauffacher, C. V., Hallenga, K. & Van Etten, R. L. (2005). *Protein Sci.* **14**, 2515–2525.
Hagelueken, G., Huang, H., Mainprize, I. L., Whitfield, C. & Naismith, J. H. (2009). *J. Mol. Biol.* **392**, 678–688.
Janin, J., Miller, S. & Chothia, C. (1988). *J. Mol. Biol.* **204**, 155–164.
Kabsch, W. (2010). *Acta Cryst.* D**66**, 125–132.
Kleanthous, C. (2000). Editor. *Protein–Protein Recognition.* Oxford University Press.
Kolot, M., Gorovits, R., Silberstein, N., Fichtman, B. & Yagil, E. (2008). *Virology*, **375**, 383–390.
Krissinel, E. & Henrick, K. (2007). *J. Mol. Biol.* **372**, 774–797.
Lacour, S., Bechet, E., Cozzone, A. J., Mijakovic, I. & Grangeasse, C. (2008). *PLoS One*, **3**, e3053.
Lescop, E., Hu, Y., Xu, H., Hu, W., Xia, B. & Jin, C. (2006). *J. Biol. Chem.* **281**, 19570–19577.
Long, F., Vagin, A. A., Young, P. & Murshudov, G. N. (2008). *Acta Cryst.* D**64**, 125–132.
Madhurantakam, C., Rajakumara, E., Mazumdar, P. A., Saha, B., Mitra, D., Wiker, H. G., Sankaranarayanan, R. & Das, A. K. (2005). *J. Bacteriol.* **187**, 2175–2181.
Mansfield, J., Genin, S., Magori, S., Citovsky, V., Sriariyanum, M., Ronald, P., Dow, M., Verdier, V., Beer, S. V., Machado, M. A., Toth, I., Salmond, G. & Foster, G. D. (2012). *Mol. Plant Pathol.* **13**, 614–629.
Morona, J. K., Morona, R. & Paton, J. C. (2006). *Proc. Natl Acad. Sci. USA*, **103**, 8505–8510.
Musumeci, L., Bongiorni, C., Tautz, L., Edwards, R. A., Osterman, A., Perego, M., Mustelin, T. & Bottini, N. (2005). *J. Bacteriol.* **187**, 4945–4956.
Nath, S., Banerjee, R. & Sen, U. (2014). *Biochem. Biophys. Res. Commun.* **450**, 390–395.
Nimtz, M., Mort, A., Domke, T., Wray, V., Zhang, Y., Qiu, F., Coplin, D. & Geider, K. (1996). *Carbohydr. Res.* **287**, 59–76.
O'Riordan, K. & Lee, J. C. (2004). *Clin. Microbiol. Rev.* **17**, 218–234.
Ostanin, K., Pokalsky, C., Wang, S. & Van Etten, R. L. (1995). *J. Biol. Chem.* **270**, 18491–18499.
Raugei, G., Ramponi, G. & Chiarugi, P. (2002). *Cell. Mol. Life Sci.*, **59**, 941–949.
Robert, X. & Gouet, P. (2014). *Nucleic Acids Res.* **42**, W320–W324.
Soulat, D., Vaganay, E., Duclos, B., Genestier, A. L., Etienne, J. & Cozzone, A. J. (2002). *J. Bacteriol.* **184**, 5194–5199.
Stehle, T., Sreeramulu, S., Löhr, F., Richter, C., Saxena, K., Jonker, H. R. & Schwalbe, H. (2012). *J. Biol. Chem.* **287**, 34569–34582.
Su, X.-D., Taddei, N., Stefani, M., Ramponi, G. & Nordlund, P. (1994). *Nature (London)*, **370**, 575–578.
Tabernero, L., Aricescu, A. R., Jones, E. Y. & Szedlacsek, S. E. (2008). *FEBS J.* **275**, 867–882.
Tabernero, L., Evans, B. N., Tishmack, P. A., Van Etten, R. L. & Stauffacher, C. V. (1999). *Biochemistry*, **38**, 11651–11658.
Temel, D. B., Dutta, K., Alphonse, S., Nourikyan, J., Grangeasse, C. & Ghose, R. (2013). *J. Biol. Chem.* **288**, 15212–15228.
Tipton, K. F., Armstrong, R. N., Bakker, B. M., Bairoch, A., Cornish-Bowden, A., Halling, P. J., Hofmeyr, J., Leyh, T. S., Kettner, C., Raushel, F. M., Rohwer, J., Schomburg, D. & Steinbeck, C. (2014). *Perspect. Sci.* **1**, 131–137.
Vanneste, J. L. (2000). *Fire Blight.* New York: CABI Publishing.
Vega, C., Chou, S., Engel, K., Harrell, M. E., Rajagopal, L. & Grundner, C. (2011). *J. Mol. Biol.* **413**, 24–31.
Walton, K. M. & Dixon, J. E. (1993). *Annu. Rev. Biochem.* **62**, 101–120.
Wang, S., Tabernero, L., Zhang, M., Harms, E., Van Etten, R. L. & Stauffacher, C. V. (2000). *Biochemistry*, **39**, 1903–1914.
Wuerges, J., Caputi, L., Cianci, M., Boivin, S., Meijers, R. & Benini, S. (2015). *J. Struct. Biol.* **191**, 290–298.
Xu, H., Xia, B. & Jin, C. (2006). *J. Bacteriol.* **188**, 1509–1517.
Yuvaniyama, J., Denu, J. M., Dixon, J. E. & Saper, M. A. (1996). *Science*, **272**, 1328–1331.
Zabell, A. P., Schroff, A. D. Jr, Bain, B. E., Van Etten, R. L., Wiest, O. & Stauffacher, C. V. (2006). *J. Biol. Chem.* **281**, 6520–6527.
Zhang, M., Stauffacher, C. V., Lin, D. & Van Etten, R. L. (1998). *J. Biol. Chem.* **273**, 21714–21720.
Zhang, M., Stauffacher, D. L. & Van Etten, R. L. (1995). *Advances In Protein Phosphatases*, Vol. 9, edited by W. Merlevede, pp. 1–23. Leuven University Press.
Zhang, M., Van Etten, R. L. & Stauffacher, C. V. (1994). *Biochemistry*, **33**, 11097–11105.
Zhang, M., Zhou, M., Van Etten, R. L. & Stauffacher, C. V. (1997). *Biochemistry*, **36**, 15–23.
Zhang, Z., Harms, E. & Van Etten, R. L. (1994). *J. Biol. Chem.* **269**, 25947–25950.
Zhang, Z.-Y. & Dixon, J. E. (1994). *Adv. Enzymol. Relat. Areas Mol. Biol.* **68**, 1–36.
Zhang, Z.-Y. & Van Etten, R. L. (1991). *Biochemistry*, **30**, 8954–8959.
Zhang, Z.-Y., Wang, Y. & Dixon, J. E. (1994). *Proc. Natl Acad. Sci. USA*, **91**, 1624–1627.